1 **Repurposing of Berbamine Hydrochloride to Inhibit Ebola Virus by Targeting**

2 **Viral Glycoprotein**

3 **Dongrong Yi[1#], Quanjie Li[1#], Xiangguo Qiu[2#], Han Wang[3], Zhenlong Liu[4], Shihua He[2], Wenjun Zhu[2], Kai Lv[1],**

4 **Xiangyang Chi[2,5], Ling Ma[1], Yujia Wang[1], Jing Wang[1], Yongxin Zhang[1], Cong Zeng[6], Mingliang Liu[1], Shanlv**

5 **Liu[6], Chen Liang[4], Xiaoyu Li[1], Logan Banadyga[2*], Yi Shi[3, 7*], George F. Gao[3, 7], Rongtuan Lin[4], Shan Cen[1*]**

6 [1] Institute of Medicinal Biotechnology, Chinese Academy of Medical Sciences and Peking Union Medical School,
7   Beijing 100050, China;

8 [2] Special Pathogens Program, National Microbiology Laboratory, Public Health Agency of Canada, Winnipeg, MB R3E
9   3R2, Canada

10 [3] CAS Key Laboratory of Pathogenic Microbiology and Immunology, Institute of Microbiology, Chinese Academy of
11   Sciences, Beijing 100101, China;

12 [4] Lady Davis Institute, Jewish General Hospital, McGill University, Montreal, Quebec, Canada;

13 [5] Laboratory of Vaccine and Antibody Engineering, Beijing Institute of Biotechnology, Beijing, China

14 [6] Center for Retrovirus Research, The Ohio State University, Columbus, Ohio, USA;

15 [7] University of Chinese Academy of Sciences, Beijing 100049, China;

16 * Correspondence: shancen@imb.pumc.edu.cn (S.C.); shiyi@im.ac.cn (Y.S.); logan.banadyga@canada.ca (L.B.)

17 [#] These authors contributed equally to this work.

18

19 **Ebola virus (EBOV) infection leads to staggeringly high mortality rates. Effective and low-cost treatments**

20 **are urgently needed to control frequent EBOV outbreaks in Africa. In this study, we report that a natural**

21 **compound called berbamine hydrochloride strongly inhibits EBOV replication *in vitro* and *in vivo*. Our**

22 **work further showed that berbamine hydrochloride acts by direct binding to the cleaved EBOV**

23 **glycoprotein (GPcl), disrupting GPcl interaction with viral receptor NPC1, thus blocking the fusion of viral**

24 **and cellular membranes. Our data support the probability of developing anti-EBOV small molecule drugs**

25 **by targeting viral GPcl. More importantly, since berbamine hydrochloride has been used in clinic to treat**

26 **leukopenia, it holds great promise of being quickly repurposed as an anti-EBOV drug.**

29

30

Ebola virus (EBOV) and Marburg virus (MARV) are highly pathogenic. Both viruses belong to the *Filoviridae*, and cause acute hemorrhagic fever in humans with high fatality rates[1, 2]. The recent EBOV outbreak (2014–2016) in West Africa claimed over 11 000 lives. However, there is currently no licensed small-molecule drug to treat or prevent EBOV infection, making EBOV a severe public health threat with the possibility of causing a global pandemic[2]. EBOV is a negative-sense enveloped RNA virus. The virus particle is decorated with glycoprotein (GP)[3], which is solely responsible for virus entry[4-6]. GP exists as a trimer, and each monomer consists of two subunits, GP1 and GP2. Following internalization at the cell surface, EBOV transports to the late endosomes where the glycan cap sheathing the receptor-binding region of GP1 is removed by endosomal cathepsin[7]. Thus primed GP (cleaved GP, GPcl) interacts with the endosomal protein Niemann-Pick C1 (NPC1) and triggers the fusion of viral and endosomal membranes[8-12]. Given the crucial role of GP in viral entry, it has become a primary target for the development of anti-EBOV therapies[13, 14].

Indeed, a number of small molecule compounds have been tested for inhibition of EBOV GP-mediated virus entry through targeting GP and cellular proteins including cathepsin, NPC1, kinase/phosphatase, ion channel, and G protein-coupled receptor (15-23). We previously identified small peptides that structurally mimic the GPcl-binding region in NPC1 and specifically inhibit EBOV entry (24). However, one potential drawback of inhibiting a cellular target is the risk of toxicity, which often deters use of such drugs in the clinic. We now report a small molecule with potent anti-EBOV activity that is able to target the receptor-binding site in GPcl.

Identification of berbamine hydrochloride as an EBOV entry inhibitor.

We previously characterized the NPC1-binding site in GPcl, consisting of residues V79, T83, K84, F88, I113, V141, and P146 (24) (Fig. 1a). Based on this result, we designed a virtual screening strategy, as shown in Fig.1b, and systematically examined 4114 compounds from the focused small compound libraries, and ranked these compounds based on the predicted binding free energies (ΔG_{ADV}). A total of 334 compounds had a ΔG_{ADV} lower than -9.0 kcal/mol (Extended Data Fig. S1) and were further visually inspected for H-bond, π-π, or salt bridge interactions to discard unrealistic poses with unreasonably high score. A final list of 46 compounds (Extended Data Table. S1) were selected for further study.

We first assessed the inhibitory effect of the selected 46 compounds on infection of HIV-Luc reporter virus that was pseudotyped with EBOV GP (EBOV pseudoparticle, EBOVpp) or vesicular stomatitis virus (VSV) GP (VSV pseudoparticle, VSVpp), as we described previously (24). Of these 46 compounds, EEI-10 (Fig. 1c), EEI-33 and EEI-45 (Extended Data Fig. S2) exhibited more than 80% inhibition of EBOVpp infection, but less than 20% reduction in VSVpp infectivity, which suggests that these three compounds selectively block EBOV GP-mediated viral entry. Such a selective inhibition was also observed for the known EBOV entry inhibitor tetrandrine (thereafter called TET) (17). Next, we determined the binding affinity of the selected compounds to the purified GPcl *in vitro* in the BLI binding assay. The association and dissociation data suggest that only

68 EEI-10 and EEI-20 interacted directly with GPcl with a KD of 217 µM and 229 µM, respectively (Fig. 1d and

69 Extended Data Fig. S3). Together, among the 46 compounds tested, only EEI-10 both binds to GPcl and

70 selectively inhibits EBOV GP-mediated viral entry.

71

72 EEI-10, also called berbamine hydrochloride, is a natural compound extracted from the berberis amurensis

73 and has been used in the clinic to treat leukopenia (*25*). Repurposing of an approved drug to inhibit EBOV

74 represents a great opportunity of developing new anti-EBOV drugs. We thus decided to further characterize

75 EEI-10 inhibition of EBOV. First, we observed that EEI-10 profoundly inhibited EBOVpp but not VSVpp (Fig.

76 1e). Results of dose-response experiments revealed a concentration-dependent inhibition of EBOVpp in

77 293T cells with EC_{50} of 0.49 µM (Fig. 1f). No cytotoxic effect of EEI-10 was observed even at 10 µM (Extended

78 Data Fig. S4a). Importantly, EEI-10 potently suppressed EBOV infection of Vero E6 cells (EC_{50}=4.1 µM, EC_{90}

79 =7.6 µM) (Fig. 1g), and did not affect cell viability at the concentrations used (Extended Data Fig. S4b). These

80 data together suggest that EEI-10 is a potent EBOV inhibitor.

81
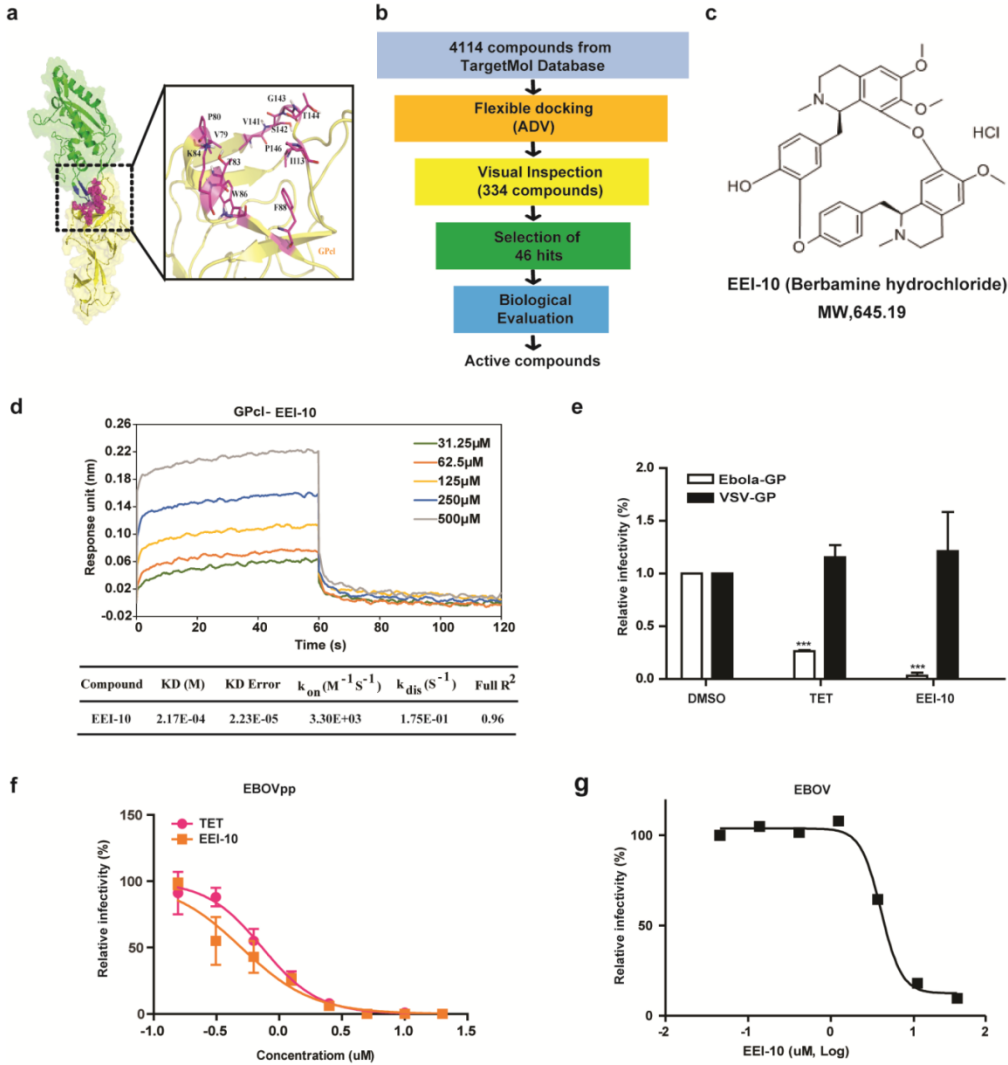
83 **Fig.1 Identification of EEI-10 as an EBOV entry inhibitor.** a, The receptor binding region identified in GPcl (PDB ID 5F1B).

84 Left, the structure of the GPcl (yellow) in complex with NPC1 (green). Right, the receptor binding cavity at the top of GPcl.

85 Highlighted in magenta is residues that constitute the interaction interface and are targeted by the virtual screening. b,

86 The virtual screening strategy designed to identify small molecules targeting GPcl. c, Chemical structure of EEI-10, with

87 molecule weight (MW). d, Representative association and dissociation sensorgrams of EEI-10 binding to EBOV-GPcl.

88 Values of KD, KD Error, kon, kdis, and R2 are presented. e, HEK293T cells were infected with the EBOVpp in the presence

89 of EEI-10 at the final concentration of 10 μM. VSVpp was used to control the specific antiviral effect of the tested drugs.

90 Data are normalized to that of the control group (arbitrarily set as 1), and shown as means ± s.d. n = 3. f, Does-depended

91 inhibition of EBOVpp by EEI-10 or TET. g, Inhibition of EBOV infection of Vero E6 cells by EEI-10 of different doses. EC50

92 and EC90 values were calculated by GraphPad Prism 5.0. Data shown are means ± s.d. n = 3. P values were calculated

93 using a two-sided paired t-test.

94

95 ***EEI-10 inhibits EBOV GP-mediated fusion of viral and cellular membranes.***

96 To determine whether EEI-10 inhibits EBOV GP-mediated virus entry, we first performed a time-of-addition

97 experiment using EBOVpp. EEI-10 was added at different time points before and after EBOVpp infection. The

98 results showed that both EEI-10 and TET markedly inhibited viral infection at the early time points of drug

99 addition, and their inhibitory effects decreased after 4 hpi (Fig. 2a). In contrast, the HIV-1 reverse

100 transcriptase inhibitor efavirenz (EFV) maintained its inhibitory effect up to 8 hpi. We further measured the

101 possible effect of EEI-10 on the internalization of EBOVpp from the cell surface by quantifying the uptake of

102 viral genomic RNA, and observed no effect as opposed to the marked inhibition by heparin (Fig. 2b), which

103 has been shown to block the early attachment of EBOV to the target cells (*26*). These data support that

104 EEI-10 inhibits an early step of EBOVpp infection, after EBOV GP-mediated internalization from the cell

105 surface but prior to viral RNA replication.

106

107 It is known that following internalization at the cell surface, EBOV particles translocate to the acidic late

108 endosomes where virus-cell membrane fusion occurs, leading to the release of viral RNA into the

109 cytoplasm(*27, 28*). Imaging EBOVpp-infected cell at 4 hpi revealed a similar number of virions in the LAMP1

110 (lysosomal associated membrane protein 1)-positive late endosome/lysosome compartments in cells treated

111 with either EEI-10 or control DMSO (Fig. 2c and Extended Data Fig. S5). This further supports the data in

112 Figure 2b that EEI-10 does not affect the early events of virus entry from uptake of virus at the cell surface to

113 trafficking of virions to the acidic compartments. We next tested whether the fusion of viral and cellular

114 membranes is inhibited by EEI-10 using a beta-lactamase-Vpr chimeric protein (BlaM-Vpr) release assay that

115 has been established to measure the delivery of HIV-1 core into the cytoplasm(*29*). We found that EEI-10

116 significantly reduced the cytoplasmic entry of BlaM-Vpr from EBOVpp by approximate 80%, whereas no such

117 effect of EEI-10 was observed for VSVpp (Fig. 2d and Extended Data Fig. S6). This suggests that EEI-10

118 specifically inhibits the delivery of BlaM-Vpr into the cytoplasm resulting from EBOV GP-mediated

119 membrane fusion. In further support of this conclusion, adding MG132 to cell culture for preventing the

120 degradation of incoming virion, a pronounced increase was detected in the level of EBOVpp particles in

121 newly infected cells treated with either EEI-10 or TET, but not for VSVpp infection (Fig. 2e and Extended Data

122 Fig. S7), suggesting that EEI-10-mediated delay of virus entry at the late endosomes causes accumulation of

123 EBOVpp particles.

124

125
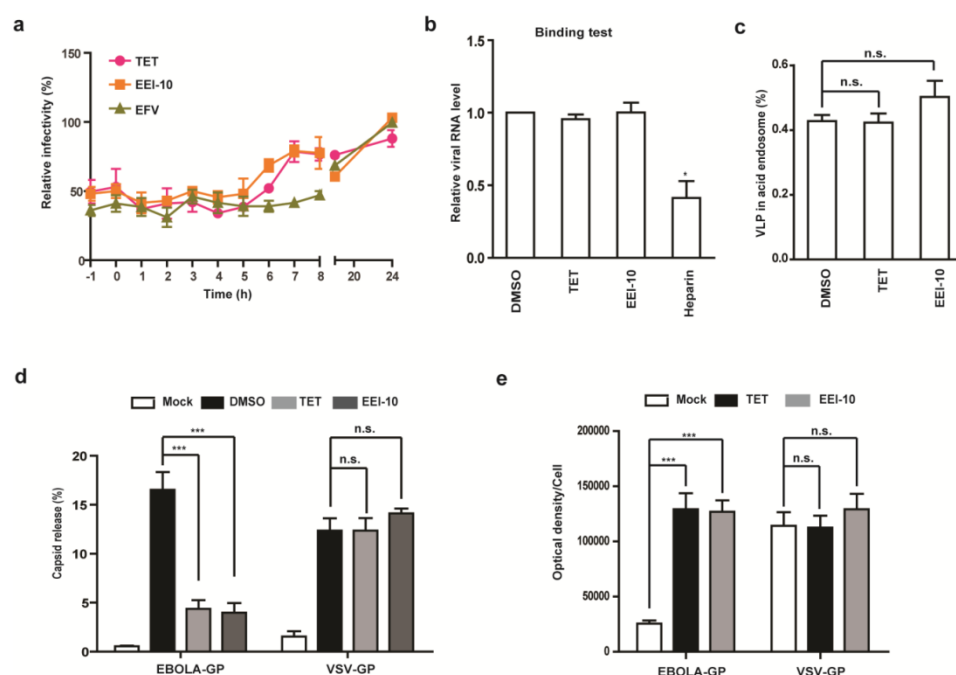
126 **Fig. 2 EEI-10 inhibits EBOV-GP dependent virus-cell membrane fusion.** a, Time-addition experiment to determine the

127 inhibition mechanism by EEI-10, TET and efavirenz (EFV). Data shown are the means ± s.d. n = 3. b, Binding test to

128 measure the effect of EEI-10 on virus binding to the cell membrane. Heparin was used as a positive control. Viral RNA

129 from virus particles binding to the cell membrane was quantified by qRT-PCR. Data are normalized to that the control

130 group which is arbitrarily set to 1. c, Virus particles (red) in the acidic endosomes were scored by their colocalization with

131 Lamp1 (green) (as for fig. S5). Fluorescence intensity of green and red signals from randomly selected cells (n≥30) was

132 quantified by Image-Pro Plus 10 software. d, VLPs (EBOVpp and VSVpp) loaded with BlaM-Vpr were used to measure

133 membrane fusion and virus capsid release into the cytoplasm after EEI-10 and TET treatment by flow cytometry (as for

134 fig. S6). The bar graph presents the percentages of virus release into the cytoplasm. Data shown are the means ± s.d. n =

135 3. e, VLPs (EBOVpp and VSVpp) accumulated in the cytoplasm after EEI-10 and TET treatment. The number of VLPs (red

136 signals) in confocal images was determined from randomly selected cells (n≥80). The fluorescence intensity was

137 quantified by Image-Pro Plus 10 software. P values were calculated using a two-sided paired t-test.

138

139 ***EEI-10 disrupts binding of EBOV GPcl to NPC1.***

140 We next determined whether EEI-10 inhibits EBOV GP-mediated entry by disrupting the binding of GP to its

141 receptor NPC1 in the infected cell. We first observed that that EEI-10 treatment reduced the colocalization

142 of EBOVpp particles with NPC1 in the infected cells (Fig. 3a), as opposed to TET which targets the two-pore

143 channels and had no effect as previously reported (*17*). EBOV GP can only bind to NPC1 after cleavage by the

144 endosomal cathepsin. We thus pretreated EBOVpp with the protease thermolysin, which completes GP

145 cleavage(*8*), and then infected cells in the presence of EEI-10. Again, strong inhibition was observed with

146 EEI-10 but not with cysteine protease inhibitor E-64 (Fig. 3b). Thus, EEI-10 diminishes the colocalization of

147 EBOVpp with NPC1 not through affecting GP proteolysis. We next performed co-immunoprecipitation to

148 measure the association of GPcl with its receptor NPC1 and found that EEI-10, but not TET, markedly

149 reduced GPcl-NPC1 interaction (Fig. 3c). This observation was supported by the data of proximity ligation

150 assay (PLA), showing that treatment with EEI-10 diminished GPcl-NPC1 interaction in the infected cells by

151 approximately 80% (Fig. 3d). We further showed that EEI-10 did not affect the cellular content of cholesterol

152 (Extended Data Fig. S8) in contrast with NPC1 inhibitors U18666A and compound 3.0 that inhibited EBOV

153 entry by causing cholesterol accumulation in late endosomes, suggesting that EEI-10 does not act on NPC1.

154 We thus conclude that EEI-10 binds to GPcl, prevents GPcl from binding NPC1, and inhibits GP-mediated

155 fusion of viral and cellular membranes.

156

157
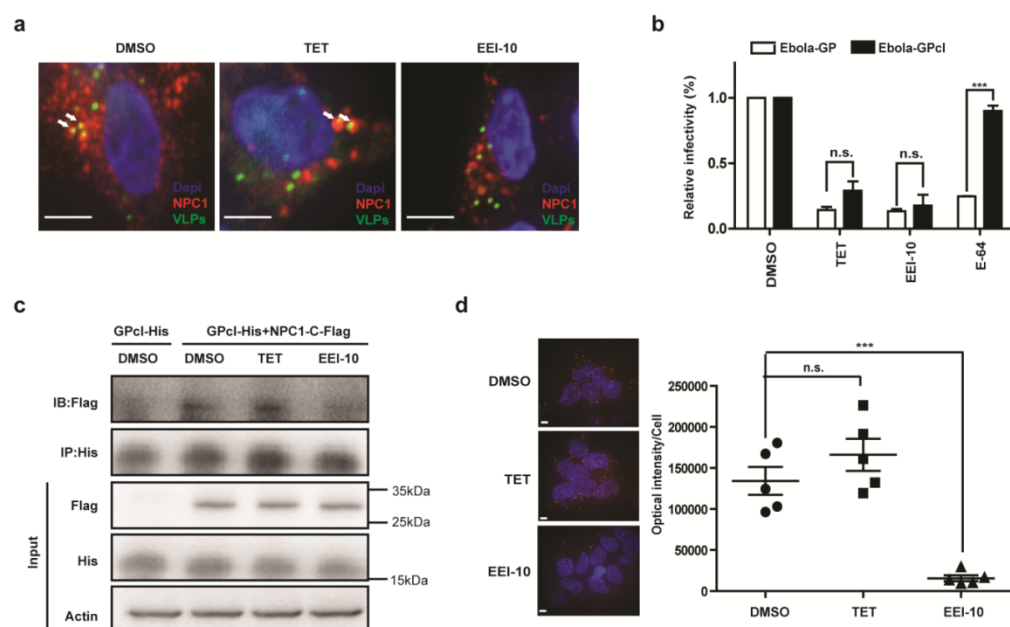
158 **Fig. 3 EEI-10 disrupts the binding of EBOV-GPcl to NPC1.** a, Colocalization of Ebola VLPs with NPC1 was determined by

159 incubating VLPs with HEK293 cells for 4 hours. Representative confocal images are shown. Colocalized Ebola VLPs (Green)

160 and NPC1(Red) were indicated by arrowheads. Scale bars, 5 μm. b, HEK293T cells were exposed to EBOVpp which were

161 treated with protease thermolysin to generate EBVO GPcl, in the presence of EEI-10 or TET. The cysteine protease

162 inhibitor E-64 was used as a positive control. Luciferase activities were measured and normalized to those of untreated

163 controls (mean ± s.d. n = 3). Each data set is representative of three independent experiments. c, Interaction between

164 NPC1-C-Flag and GPcl-His was determined with Co-IP in the presence of EEI-10 or TET. Data shown are the representative

165 of three independent experiments. d, In situ PLA to analyze the interaction between Ebola-GP (or VSV-GP) and cellular

166 NPC1 in the presence of the EEI-10 or TET. Representative confocal images are shown. Scale bars, 5 μm. Mean

167 fluorescence intensity was collected from at least 30 cells and further analyzed for each treatment.

168

169 *GPs of EBOV and MARV share a similar binding pocket for EEI-10 and are both inhibited by EEI-10.*

170   We next used the AutoDock Vian computation program to model the binding of EEI-10 to GPcl. In the

171   generated model of GPcl in complex with EEI-10 (Fig. 4a), EEI-10 is located at the hydrophobic pocket in GPcl

172   and forms hydrogen bond interaction with the amino residue E112. We further employed the MM/GBSA

173   computation approach to calculate the binding free energy of EEI-10 and decomposed the free energy at the

174   amino acid level. The cavity analysis showed that the major contributing amino acids to the binding of EEI-10

175   include E112, T83, I113, V141, F88, L111, W86, V79, P80, and G143, which are ranked based on their ΔG_{ADV}

176   in the range from -2.54 to -0.62 kcal/mol (Extended Data Table. S2).

177

178   To validate this binding model, we mutated the three top-ranking amino acids E112, T83 and I113, and

179   examined their effect on the sensitivity of EBOV GP-mediated entry to EEI-10. The E112A mutation severely

180   impaired viral infectivity, thus was not further tested for EEI-10 inhibition (Extended Data Fig. S9). The I113A

181   GP mutant was refractory to EEI-10 while remaining sensitive to the TET entry inhibitor (Fig. 4b). In the

182   meantime, the T83A mutation exerted no effect on the sensitivity of GP to either EEI-10 or TET inhibition (Fig.

183   4b); this is likely because A83 is able to restore the van der Waals interaction with EEI-10 which is observed

184   for T83 as predicted in our computation model (Extended Data Table. 2). These data demonstrate that I113

185   is a key residue in contact with EEI-10 and that its mutation leads to resistance to EEI-10, which supports the

186   structural model of GPcl binding to EEI-10.

187

188   Recent studies have revealed a common receptor-binding site in GPs of several filoviruses including EBOV

189   and MARV (*13, 30*), which suggests that EEI-10 may inhibit MARV infection as well. Indeed, EEI-10 inhibited

190   the MARV-GP/HIV-luc virus infection at an EC50 = 0.99 µM, and inhibited MARV itself at an EC50 = 4.06 µM

191   (Fig. 4c, d). We further conducted computational docking of EEI-10 to MARV-GP1 and then preformed MD

192   simulation to relax the complex. The binding free energy of the MARV GP/EEI-10 was calculated as

193   ΔG_{ADV}=-9.3kcal/mol, which is moderately higher than that of EBOV-GPcl/EEI-10 complex (ΔG_{ADV}=-10.9

194   kcal/mol). Notably, these two complexes are well superposed at the EEI-10 binding sites (Fig. 4e). The top 10

195   amino acids in MARV-GP1 that contribute most to the binding energies are L64, S67, K68, A71, F72, I95, V97,

196   I125, G127, and N129 (Extended Data Table. S3), which are equivalent to P80, T83, K84, G87, F88, L111, I113,

197   V141, G143, and G145 in EBOV GPcl. Importantly, seven of the top 10 major contributing amino residues are

198   shared in both complexes (Fig. 4f). These data suggest that EEI-10 is able to bind to the GPs of EBOV and

199   MARV, and inhibit both viruses.

200
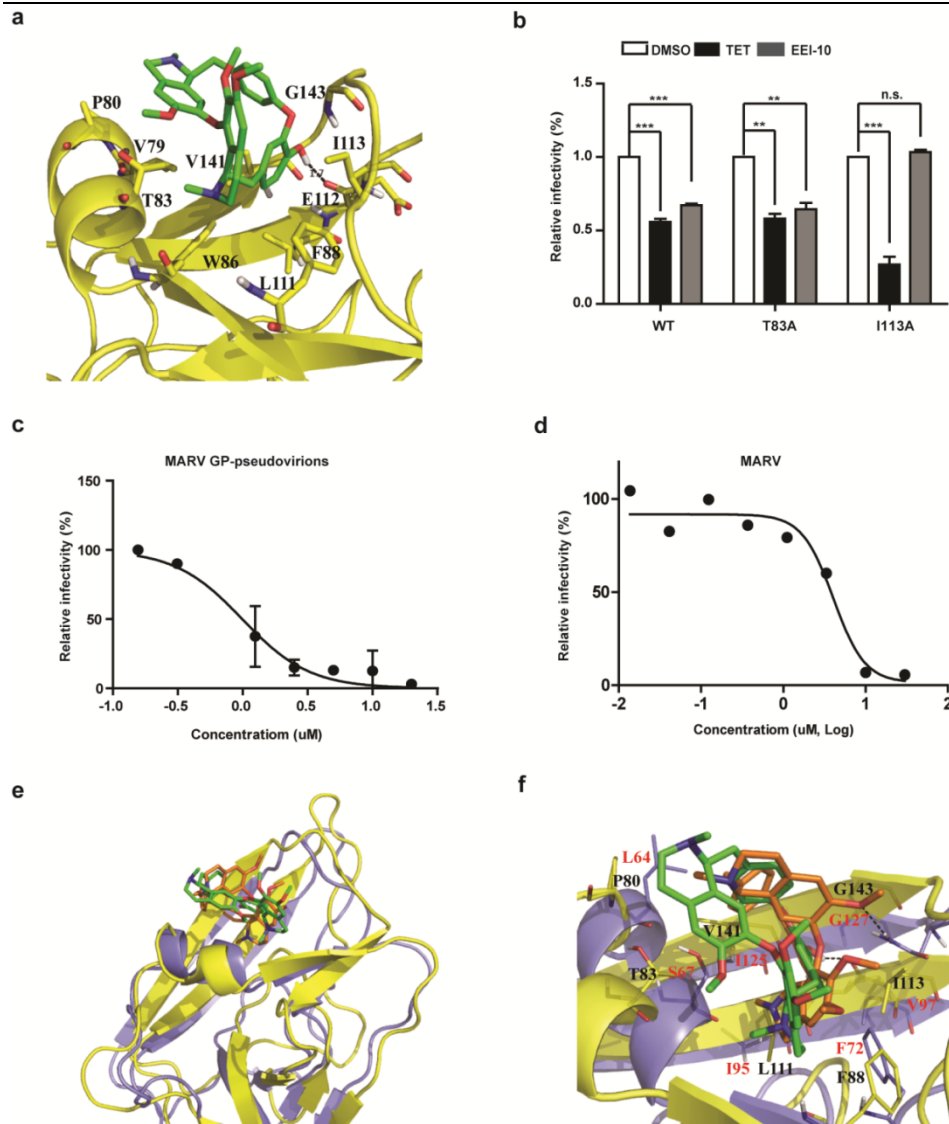
Fig. 4 EEI-10 inhibits infection mediated by the GPs of EBOV and MARV. a, Structural model of EEI-10 binding to GPcl. Amino residues (in yellow) binding to EEI-10 (in green) are shown as sticks. The oxygen, nitrogen, and hydrogen atoms are colored in red, blue, and white, respectively. For clarity, only polar hydrogen atoms are shown. The PDB ID of the EBOV-GPcl crystal structure used for molecular modeling is 5F1B. b, Inhibition of the T83A and I113A GP mutants by EEI-10. Luciferase activities were measured and normalized to those of untreated controls. Data shown are the average of three independent experiments, presented in mean ± SD. c, Inhibition of MARV GP-pseudovirions by EEI-10 of different doses. d, Different doses of EEI-10 were tested for inhibition of MARV infection in Vero E6 cells. EC50 values were calculated with GraphPad Prism 5.0. Each data point is the average of three independent experiments. e, Superposition of the structures of the EBOV-GPcl/EEI-10 and MARV-GP1/EEI-10 complexes. EBOV-GPcl and MARV-GP1 are shown as yellow and slate cartoons, and their associate inhibitor EEI-10 was shown as green and orange sticks. f, Comparison of protein–ligand interactions in the EBOV-GPcl/EEI-10 and MARV-GP1/EEI-10 complexes. Key residues in the MARV-GP1/EEI-10 binding pocket are highlighted in red. The PDB IDs of crystal structures used for molecular modeling are 5F1B for EBOV GPcl and 5UQY for MARV GP1.

EEI-10 protects mice from lethal EBOV infection.

Finally, we asked whether EEI-10 was able to protect mice from lethal EBOV infection. Mice were treated orally once per day for 6 days with 100 mg/kg EEI-10 beginning the day prior to inoculation with a lethal dose of mouse-adapted EBOV (MA-EBOV) (Fig. 5a). Remarkably, 100% of the mice treated with EEI-10 survived infection while only one of the PBS-treated animals survived (Fig. 5b), although all exhibited weight loss (Fig. 5c). To determine whether EEI-10 was also effective if treatment was begun post-infection, mice were again inoculated with MA-EBOV and then treated orally with the same dose of drug beginning at 1 day post-infection for a period of 6 days. Whereas all PBS-treated mice succumbed to infection by day 7, nearly all mice treated with EEI-10 survived, and the time to death was prolonged in the single treated animal that died (Fig. 5d). Again, all animals exhibited weight loss (Fig. 5e), suggesting that, while EEI-10 treatment provided a significant survival advantage, it did not prevent some signs of disease.
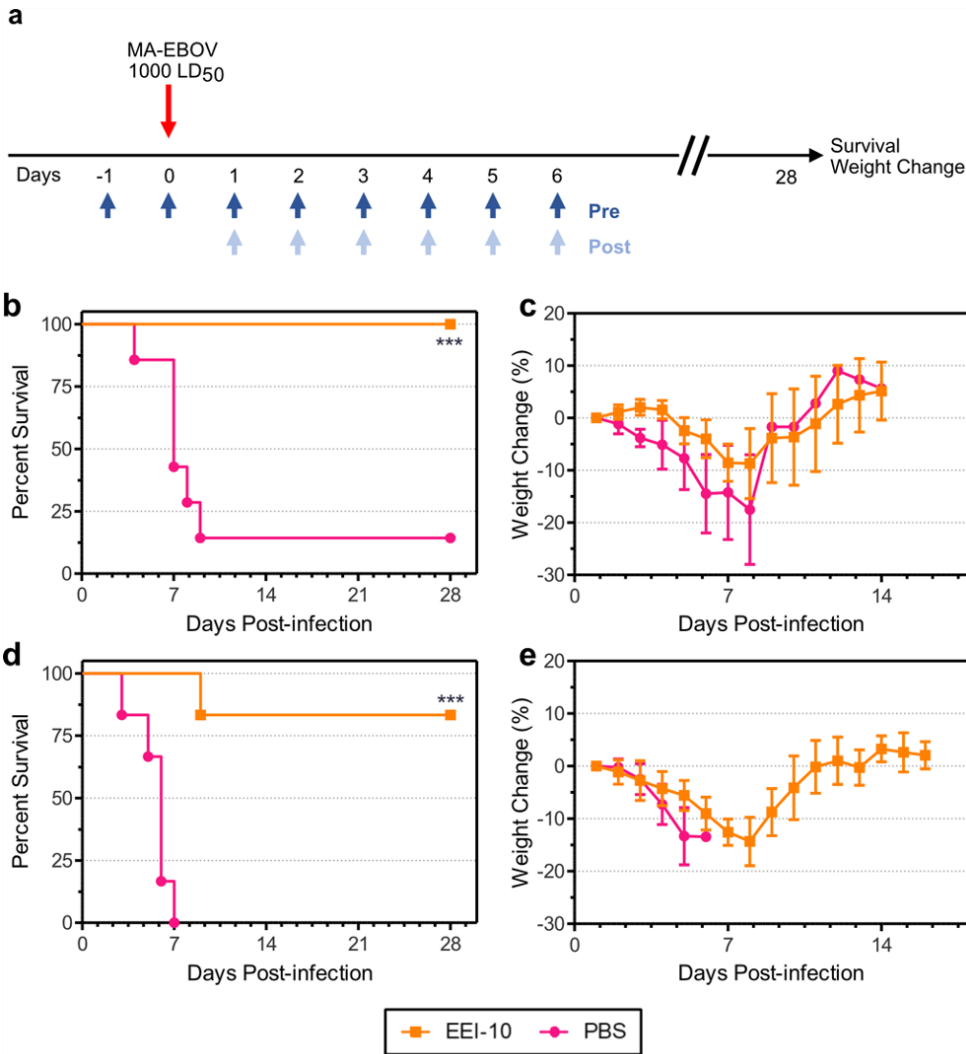
Fig. 5. EEI-10 prevents lethal EBOV infection in mice. a, Schematic representation of EEI-10 treatment protocol and EBOV infection of mice. b,c, Balb/c mice were treated orally with EEI-10 (100 mg/kg; n = 10) or PBS (n = 7) one day before infection with 1000 LD50 mouse-adapted EBOV (MA-EBOV). Treatment continued once daily until day 6 after infection.

232   Survival (in b) and average percent weight change ± standard deviation (in c) are shown. d,e, Balb/c mice were infected

233   with 1000 LD50 MA-EBOV one day prior to oral treatment with EEI-10 (100 mg/kg; n = 6) or PBS (n = 6). Treatment

234   continued once daily until day 6 post-infection. Survival (in d) and average percent weight change ± standard deviation

235   (in e) are shown Survival curves were compared using the Log-rank Test; ***, p ≤ 0.001.

236

237   This remarkable protective efficacy of EEI-10 may be partially attributed to the relatively weak interaction of

238   GPcl with its receptor NPC1. With a KD of 158 μM, as measured *in vitro* using recombinant proteins (31), the

239   interaction between these two proteins was likely easily disrupted by EEI-10. Through medicinal chemistry

240   to modify EEI-10 and select for variants with greater affinity to GPcl, we expect to identify EEI-10 derivatives

241   exhibiting much stronger inhibition of EBOV as well as a higher genetic barrier to deter the development of

242   viral resistance. Additionally, as a drug to treat leukopenia, EEI-10 is expected to modulate certain cellular

243   pathways and host immunity, which may have also contributed to its protection of mice against lethal EBOV

244   infection.

245

246   Of note, EEI-10 was demonstrated to bind to EBOV GPcl and potently inhibit virus entry, whereas *in vitro*

247   binding assay revealed that EEI-10 exhibited a low affinity for GPcl, with KD values above 100 μM (Fig. 1d),

248   likely due to the inability of the molecule to fit into and fully fill the extremely large receptor binding cavity

249   (Fig. 1a). Nevertheless, a similar affinity (KD = 158 μM) was reported in the complex structure of GPcl bound

250   to NPC1(*31*), suggesting the feasibility of EEI-10 to compete with NPC1 for binding to GPcl. Moreover, lower

251   pH was reported to enhance the interaction between GPcl and NPC1(*9*). This implies that the binding affinity

252   of EEI-10 in the acidic endosome where it occurs may be underrated *in vitro*.

253

254   In summary, we have identified a natural compound berbamine hydrochloride (EEI-10) that potently inhibits

255   EBOV infection of cultured cells through direct binding to viral GPcl and impairing the interaction of GPcl

256   with the viral receptor NPC1. Our data further showed that EEI-10 strongly inhibits another pathogenic

257   filovirus, MARV, implicating the potential use of EEI-10 as a broad-spectrum inhibitor of filovirus infection.

258   Given that berbamine hydrochloride is already approved to treat leukopenia and has been thoroughly

259   evaluated for its safety and pharmacokinetics properties, this drug holds great promise for saving the lives of

260   EBOV patients and preventing future EBOV epidemics or pandemics.

261

Conflicts of Interest: The authors declare no conflict of interest.

Methods

Cell lines, Plasmids and Virus

HEK293T, Vero E6 and HeLa cells were obtained from the American Type Culture Collection and maintained at 37°C and 5% CO_2 in DMEM supplemented with 10% HI-FBS, 2 mM L-glutamine, 50 U/ml penicillin, and 50 ug/ml streptomycin. Plasmids encoding EBOV-GP, vesicular stomatitis virus envelope protein (VSV-GP) and HIV-l luciferase reporter vector pNL4-3.Luc.R-E- were kept in the Institute of Medicinal Biotechnology, Beijing. The GP genes of MARV (GenBank Accession No. ABA87127.1, amino acid (a.a.) 5941-7986) were synthesized by Suzhou GENEWIZ Biotechnology Co., Ltd., and inserted into pcDNA3.1(+) vector (Invitrogen). Plasmids encoding Vpr-Blam was kindly provided by Dr. Xu Tan (Tsinghua University, China). All work with recombinant EBOV expressing EGFP (Ebola virus H.Sapiens-rec/GIN/2014/Makona-Guekedou-C07-EGFP), mouse-adapted EBOV variant Mayinga(*32*) and wild type MARV variant Angola (Marburg virus H.spaiens-tc/AGO/2005/Angola) was performed in the containment level 4 laboratories at the Canadian Science Centre for Human and Animal Health (CSCHAH), Public Health Agency of Canada, Winnipeg, MB, Canada.

Compounds and antibodies

TargetMol's small-compound library subsets (anti-virus compound library, anti-infection compound library, nature compound library, plant-sourced compound library, anti-inflammation library, and inhibitors library) were used for virtual screening. Small molecules selected from docking procedure were purchased from

298 Target Molecule Corp. Tetrandrine (TET) and efavirenz (EFV) were maintained in the Institute of Medicinal

299 Biotechnology, Beijing.. The purity of all tested compounds is more than 95%. The following antibodies were

300 used: Mouse anti-His (TA-02; ZSGB-Bio), Mouse anti-Flag (8146S; CST), rabbit anti-Flag (B1020; Biodragon),

301 Mouse anti-NPC1 (ab134113; Abcam), Mouse anti-p24 (ab9071; Abcam), Rabbit anti-p24 (produced by our

302 own lab), Mouse anti-Lamp1 (ab24170; Abcam), Mouse anti-β-actin monoclonal antibody (Abcam) and goat

303 anti-rabbit secondary antibody (Beijing zhongshan jinqiao Biotechnology). Alexa Fluor-conjugated secondary

304 antibodies were purchased from Life Technologies.

305 **Generation of recombinant HIV pseudotyped with virus glycoproteins**

306 Ebola pseudotyped viruses (EBOV-GP/HIV-luc) were produced as previously described(*24*). Pseudotyped

307 viruses bearing VSV envelope protein (VSV-G/HIV-luc) and MARV envelope protein (MARV-GP/HIV-luc) were

308 produced in a similar way.

309 **Infection assay**

310 Screening of the selected compounds using pesudotyped virus was performed in 96-well plates as previous

311 described(*24*). Briefly, cells were infected with the EBOV-GP/HIV-luc in the presence of compounds at a final

312 concentration of 10 μM. The infected cells were lysed and the anti-EBOV activity of test compounds was

313 evaluated by measuring the luciferase activities at 48 h post infection (hpi). DMSO and TET were used as

314 negative and positive controls, respectively. The VSV-G/HIV-luc was used as a control to determine the

315 specificity of compounds. The 50% effective concentration (EC50) and EC90 values were calculated by using

316 a four-parameter logistic regression in Prism 5 (GraphPad).

317

318 To analyze the retention of EBOVpp virions in newly infected cells, HEK293T cells were infected with

319 EBOV-GP/HIV-luc at an MOI of 1.0 in the presence of MG132 (4μM). After 4 h, cells were fixed in 4%

320 paraformaldehyde for 30 min on ice and virus was stained with rabbit or mouse anti-p24 antibody, followed

321 by an anti-Rabbit AlexaFluor-555 antibody or anti-mouse AlexaFluor-488 antibody. Fluorescence was

322 monitored with a confocal microscope with a 100× oil objective lens.

323

324 To assess the effect of berbamine hydrochloride on EBOV and MARV replication, Vero E6 cells were

325 pretreated with drug (0 to 200 μM) or DMSO for 1 h at 37°C and infected at a multiplicity of infection (MOI)

326 of 0.1 with EBOV expressing enhanced green fluorescent protein (EBOV-EGFP) or wild type MARV for 1 h at

327 37°C, after which the inoculum was removed and replaced with fresh medium (DMEM plus 2% FBS). Cells

328 were further incubated for 72 h in the presence of EEI-10 or DMSO. For EBOV-EGFP-infected cells

329 fluorescence was quantified on a Biotek Synergy HTX plate reader. The percent relative infectivity was

330 determined by comparing fluorescence readings of EEI-10-treated cells to those of DMSO-treated control

331 cells. For MARV-infected cells, supernatants were harvested and viral RNA was quantified, as described

332 below. The percent relative infectivity was determined by comparing the amount of viral RNA detected in

333 EEI-10 treated cells to that of DMSO-treated control cells.

qRT-PCR

For HIV-based infections, total RNA was extracted from infected cells by use of an RNA extraction kit (Tiandz). The level of viral RNA was determined by performing qRT-PCR analysis by use of a one-step SYBR PrimeScript RT-PCR kit. The primer pair (5'-TTAAGCCTCAATAAAGCTTGCC-3' and 5'-GTTCGGGCGCCACTGCTAGA-3') amplifies the LTR of HIV. Levels of cellular glyceraldehyde-3-phosphate dehydrogenase (GAPDH) RNA were amplified with primers 5'-ATCATCCCTGCCTCTACTGG-3' and 5'-GTCAGGTCCACCACTGACAC-3'; the results served as an internal control to normalize the level of HIV RNA.

For MARV infections, viral RNA was extracted from tissue culture supernatants using the QIAamp viral RNA minikit (Qiagen). Viral RNA levels were quantified by qRT-PCR using the LightCycler 480 thermal cycler (Roche) and the LightCycler 480 RNA Master Hydrolysis Probes kit (Roche) along with the following primers and probe: 1-F, 5'-GCAAAAGCATTCCCTAGTAACATGA-3'; 1-R, 5'-CACCCCTCACTATRGCGTTYTC-3'; 2-F, 5'-GCGAAGGCATTCCCTAGTAATATGA-3'; 2-R, 5'-CACCTCTTACTATGGCATTCTC-3'; probe, 5'-56-FAM/TGGCAC CAY/ZEN/AATTCAGCAAGCATAGG/ 3IABkFQ-3'. Cycling conditions were as follows: 63°C for 3 min and 95°C for 30s, then 45 cycles of 95°C for 15 s and 60°C for 30 s.

Cytotoxicity analysis

HEK293T and Vero E6 cells were seeded in 96-well plates. Following overnight incubation at 37°C, Tetrandrine and Berbamine hydrochloride were added at different concentrations used for the viral infection studies. Cells in culture media without drug served as control. At 48h, Cell Counting kit-8 (CCK-8, Beyotime, China) was used to evaluate cell viability.

Blam-Vpr releasing assay

For production of pseudotyped viruses incorporating Blam-Vpr, HEK293T cells were transfected with 6 μg of pNL4-3.Luc.R-E-, 6 μg of pEbola-GP or pVSV-GP, 3 μg of pBlam-Vpr and 1.5 μg of pAdvantage using Lipo2000 in 10-cm dishes. Culture supernatants were collected after 48 h and filtered through a 0.45 μm filter. The virus was concentrated by ultracentrifugation at 36000 rpm for 4 h pelleting through a 20% sucrose cushion or by Centrifugal Filters (100 Kd). Detection of virus capsid release into the cell cytoplasm was performed using LiveBLAzer FRET-B/G Loading Kit with CCF4-AM (Invitrogen) according to manufacturer instructions. Briefly, HeLa or SupT1 cells were seeded on 6-well plates 1 day before the assay. After preincubation with each drug for 1 h, cells were infected with EBOV-GP/HIV-luc or VSV-GP/HIV-luc for 2 h at 37°C in the presence of the drug. After loading CCF4-AM substrate, cells were fixed in 4% paraformaldehyde and Amcyan or Pacific Blue fluorescence signals were detected by FACS.

Time-of-addition experiment

Berbamine hydrochloride (1 μM), Tetrandrine (1 μM) and Efavirenz (5 nM) were added to the 293T cell culture medium before infection (-1h), during infection (0 h), and 1, 4, 5, 6, 8, 18, and 24 hpi. Viral replication was determined at 48 hpi as described above. Cell culture treated with DMSO or TET was used as

369   negative and positive control, respectively. The HIV-1 reverse transcriptase inhibitor EFV was used to
370   confirm the rationality of our assay system.

Virus binding experiment

372   For binding tests, 4×10^5 HEK293T cells were seeded in 6-well plates overnight and infected with
373   EBOV-GP/HIV-luc for 1 h at 4°C in the presence of Tetrandrine (5 µM), Berbamine hydrochloride (5 µM) and
374   Heparin (5 µg/mL), followed by washing with PBS, and virus absorption on the cell surface was quantified
375   through the measurement of viral genomic RNA by qRT-PCR.

In vitro protease cleavage of EBOV-GP/HIV-luc

377   Concentrated EBOV-GP/HIV-luc was stocked in HEPES-MES buffer (40 mM HEPES, 40 mM
378   morpholinepropanesulfonic acid, 50 mM NaCl, 0.5mM CaCl2, pH 7.5), the GP protein was cleaved by 0.5
379   mg/mLthermolysin (Promega, Madison, WI) at 37°C for 1h. The reaction was stopped by 0.5 mM EDTA and
380   protease inhibitors. The cleavage efficiencies were confirmed by immunoblotting using anti-Flag antibody.
381   Then HEK293T cells were incubated with the cleaved or uncleaved EBOV-GP/HIV-luc in the presence of the
382   drug for 48h, the luciferase activities were detected to evaluate the antiviral efficiencies of drugs.

In situ PLA

384   In situ PLA was performed using kits from Sigma Aldrich: Duolink® PLA Detection Reagents (DUO92101)
385   according to the manufacturer. Briefly, 4% paraformaldehyde-fixed samples were incubated with blocking
386   solution to saturate nonspecific binding and subsequently with primary antibodies at 37°C for 1 h.
387   Thereafter, slides were incubated for 1 h at 37°C with Duolink® PLA probes. Ligation solution was added for
388   30 min at 37°C. Ligation solution was removed with wash buffer A, and amplification solution was added for
389   100 min at 37°C and removed with wash buffer B. Finally, Duolink in situ mounting medium with DAPI was
390   added. Fluorescence was monitored with a confocal microscope with a 100× oil objective lens.

Co-IP for Ebola GPcl and NPC1

392   HEK293T cells were transfected with plasmid expressing NPC1-C-Flag using Lipo2000 in 10 cm dishes for 48 h,
393   cells were lysed by NP40 and debris was removed through centrifugation at 12000 rpm for 10 min.
394   Tetrandrine (10 µM), Berbamine hydrochloride (10 µM) were pre-incubated with GPcl-His (1 µg) for 1h
395   before mixing with cell lysate. Anti-His antibody coated beads were used to pull down GPcl-His and the
396   bound NPC1-C-Flag was detected through WB.

Analysis of intracellular cholesterol

398   Hela cells were pretreated with Tetrandrine (5 µM), Berbamine hydrochloride (5 µM), U18666A (5 µM) for
399   24h, and then cells were collected and fixed with paraformaldehyde (4%) for 30 min on ice. After three PBS
400   washes, cells were incubated with 50 µg/mL filipinⅢ complex in the dark for 1 h at RT. After three PBS
401   washes, cells were detected by FACS in the DAPI channel.

Bio-layer Interferometry (BLI) binding assay

Octet RED (ForteBio, Inc., CA, USA) was used to measure binding affinity and kinetic profile. The purified GPcl was biotinylated by EZ-Link NHS-LC-LC-Biotin (Thermo Scientific). The biotinylated GPcl (50 μg/ml) was then captured via super streptavidin (SSA) biosensors (120 sec, at 30 °C, with 1000 rpm). A duplicate set of sensors were incubated in assay buffer (0.002% Tween-20, PBS, pH=7.4) without protein for use as a background binding control. Both the ligand and reference biosensors were quenched with 5 μg/ml biotin for 1 min. For KD determinations, the binding of a dilution series of compounds was detected for 60 sec association (kon, 1/Ms) followed by 60 sec dissociation (kdis, 1/s) in parallel to the ligand biosensors and reference biosensors. Besides, blank binding cycles using buffer only were used to correct the baseline shift during the analysis. After measurements were complete, a double reference subtraction method was processed to subtract the effect of baseline drift and nonspecific binding. KD acquired from fitting into 1:1 binding model by global fitting of multiple kinetic traces and analyzed by Data Analysis 9.0 software.

Computational methods

Using Auto-Dock Vina package(*33*), structure based virtual screening was carried out over 4114 compounds in the focused database. Based on the crystal structure of GPcl in complex with the receptor, we first generated the docking parameter files using AutoDockTools-1.5.6. The grid center was located at the receptor-binding region on the head of GPcl and was designated at dimensions (x, y, and z): 34.428 Å, -17.200 Å, and -317.00 Å. The grid size was set to 24 Å, 28 Å, and 28 Å on X, Y and Z coordinates, respectively. Then we used Open Babel software to create the ligand parameter files for docking(*34*). Each compound in the library was assigned hydrogen at pH 7.4 and converted to PDBQT format. Finally, all these compounds were docked to GPcl and ranked by their calculated binding free energies (ΔG_{ADV}). The molecular dynamic simulation and MM-GBSA calculation were performed as previously described(*24, 35*).

Animal ethics statement

Animal experiments were performed in the containment level 4 laboratories at CSCHAH. All experimental protocols were reviewed and approved by the institutional Animal Care Committee in accordance with guidelines from the Canadian Council on Animal Care. All staff working on animal experiments completed education and training programs according to the standard protocols appropriate for this level of biosafety.

Efficay of berbamine hydrochloride in EBOV-infected mice

Six- to eight-week-old female BALB/c mice (Charles River) were inoculated intraperitoneally with 1,000× the 50% lethal dose (LD50) of MA-EBOV. Mice were treated with 100 mg/kg of body weight of berbamine hydrochloride via oral administration beginning on either day -1 or day +1 post-infection and continuing daily up to day 6 post-infection. Animals in the control group were treated with PBS following the same schedule. Mice were observed daily for weight change and clinical signs.

Statistical analysis

437 Data are presented as mean ± standard deviation (SD) from at least three independent experiments..

438 Statistical comparisons of the Kaplan-Meier survival curves (Fig. 5b, d) were performed using the Log-rank

439 test. p-values are indicated as follows: p≤0.05(*), p≤0.01(**), p≤0.001(***). n.s. = not significant.

440

441

442

443   **References**

444

445   1.   H. Feldmann, T. W. Geisbert, Ebola haemorrhagic fever. *The Lancet* **377**, 849-862 (2011).

446   2.   S. T. Jacob *et al.*, Ebola virus disease. *Nature reviews Disease primers* **6**, 1-31 (2020).

447   3.   V. E. Volchkov *et al.*, Recovery of infectious Ebola virus from complementary DNA: RNA editing
448   of the GP gene and viral cytotoxicity. *Science* **291**, 1965-1969 (2001).

449   4.   K. Chandran, N. J. Sullivan, U. Felbor, S. P. Whelan, J. M. Cunningham, Endosomal proteolysis of
450   the Ebola virus glycoprotein is necessary for infection. *Science* **308**, 1643-1645 (2005).

451   5.   A. Takada *et al.*, A system for functional analysis of Ebola virus glycoprotein. *Proc Natl Acad Sci*
452   *U S A* **94**, 14764-14769 (1997).

453   6.   B. Manicassamy, J. Wang, H. Jiang, L. Rong, Comprehensive analysis of ebola virus GP1 in viral
454   entry. *J Virol* **79**, 4793-4805 (2005).

455   7.   D. Dube *et al.*, The primed ebolavirus glycoprotein (19-kilodalton GP1, 2): sequence and
456   residues critical for host cell binding. *J Virol* **83**, 2883-2891 (2009).

457   8.   J. E. Carette *et al.*, Ebola virus entry requires the cholesterol transporter Niemann-Pick C1.
458   *Nature* **477**, 340-343 (2011).

459   9.   X. Gong *et al.*, Structural Insights into the Niemann-Pick C1 (NPC1)-Mediated Cholesterol
460   Transfer and Ebola Infection. *Cell* **165**, 1467-1478 (2016).

461   10.   E. H. Miller *et al.*, Ebola virus entry requires the host-programmed recognition of an
462   intracellular receptor. *EMBO J* **31**, 1947-1960 (2012).

463   11.   D. Dube *et al.*, Cell adhesion-dependent membrane trafficking of a binding partner for the
464   ebolavirus glycoprotein is a determinant of viral entry. *Proc Natl Acad Sci U S A* **107**,
465   16637-16642 (2010).

466   12.   T. Hoenen, A. Groseth, H. Feldmann, Therapeutic strategies to target the Ebola virus life cycle.
467   *Nature Reviews Microbiology* **17**, 593-606 (2019).

468   13.   Z. A. Bornholdt *et al.*, Host-Primed Ebola Virus GP Exposes a Hydrophobic NPC1
469   Receptor-Binding Pocket, Revealing a Target for Broadly Neutralizing Antibodies. *MBio* **7**,
470   e02154-02115 (2016).

471   14.   K. A. Howell *et al.*, Antibody Treatment of Ebola and Sudan Virus Infection via a Uniquely
472   Exposed Epitope within the Glycoprotein Receptor-Binding Site. *Cell Rep* **15**, 1514-1526
473   (2016).

474   15.   E. Picazo, F. Giordanetto, Small molecule inhibitors of ebola virus infection. *Drug Discov Today*
475   **20**, 277-286 (2015).

476   16.   M. A. Trad *et al.*, Ebola virus disease: An update on current prevention and management
477   strategies. *J Clin Virol* **86**, 5-13 (2017).

478   17.   Yasuteru Sakurai *et al.*, Two-pore channels control Ebola virus host cell entry and are drug
479   targets for disease treatment. *Science* **347**, 995-998 (2015).

480   18.   H. Cheng *et al.*, Inhibition of Ebola and Marburg Virus Entry by G Protein-Coupled Receptor
481   Antagonists. *J Virol* **89**, 9932-9938 (2015).

482   19.   A. Basu *et al.*, Identification of a small-molecule entry inhibitor for filoviruses. *J Virol* **85**,
483   3106-3119 (2011).

484   20.   X. Zhang *et al.*, Characterization of the inhibitory effect of an extract of Prunella vulgaris on
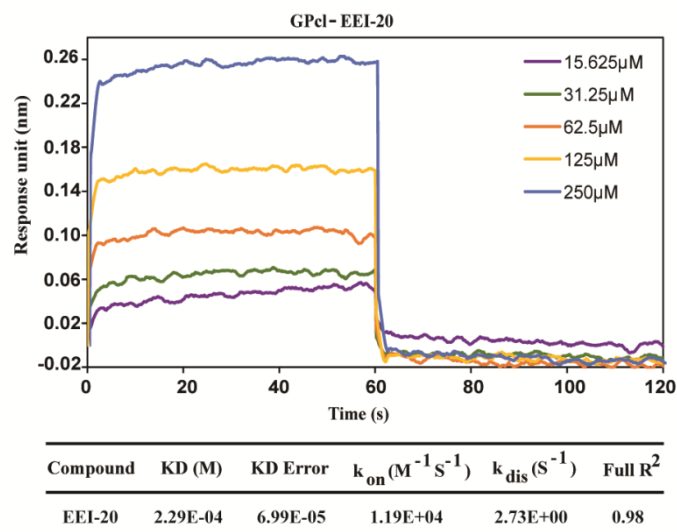
485   Ebola virus glycoprotein (GP)-mediated virus entry and infection. *Antiviral Res* **127**, 20-31
486   (2016).

487 21.   J. Ren, Y. Zhao, E. E. Fry, D. I. Stuart, Target Identification and Mode of Action of Four
488   Chemically Divergent Drugs against Ebolavirus Infection. *J Med Chem* **61**, 724-733 (2018).

489 22.   Y. Zhao *et al.*, Toremifene interacts with and destabilizes the Ebola virus glycoprotein. *Nature*
490   **535**, 169-172 (2016).

491 23.   M. Côté *et al.*, Small molecule inhibitors reveal Niemann–Pick C1 is essential for Ebola virus
492   infection. *Nature* **477**, 344-348 (2011).

493 24.   Q. Li *et al.*, Novel cyclo-peptides inhibit Ebola pseudotyped virus entry by targeting primed GP
494   protein. *Antiviral Res* **155**, 1-11 (2018).

495 25.   X. Zhang *et al.*, Treatment of Chemotherapy Related Leukocytopenia by Oral Administration of
496   Multiple Leucogenic Drugs Combined with G-CSF: an Experimental Study. *Chin J Integr Med* **35**,
497   860-865 (2015).

498 26.   A. O'Hearn *et al.*, Role of EXT1 and Glycosaminoglycans in the Early Stage of Filovirus Entry. *J
499   Virol* **89**, 5441-5449 (2015).

500 27.   M. F. Saeed, A. A. Kolokoltsov, T. Albrecht, R. A. Davey, Cellular entry of ebola virus involves
501   uptake by a macropinocytosis-like mechanism and subsequent trafficking through early and
502   late endosomes. *PLoS pathogens* **6**, e1001110 (2010).

503 28.   A. Nanbo *et al.*, Ebolavirus is internalized into host cells via macropinocytosis in a viral
504   glycoprotein-dependent manner. *PLoS pathogens* **6**, e1001121 (2010).

505 29.   M. Cavrois, C. De Noronha, W. C. Greene, A sensitive and specific enzyme-based assay
506   detecting HIV-1 virion fusion in primary T lymphocytes. *Nature biotechnology* **20**, 1151-1154
507   (2002).

508 30.   T. Hashiguchi *et al.*, Structural basis for Marburg virus neutralization by a cross-reactive human
509   antibody. *Cell* **160**, 904-912 (2015).

510 31.   H. Wang *et al.*, Ebola Viral Glycoprotein Bound to Its Endosomal Receptor Niemann-Pick C1.
511   *Cell* **164**, 258-268 (2016).

512 32.   M. Bray, K. Davis, T. Geisbert, C. Schmaljohn, J. Huggins, A mouse model for evaluation of
513   prophylaxis and therapy of Ebola hemorrhagic fever. *The Journal of infectious diseases* **178**,
514   651-661 (1998).

515 33.   O. Trott, A. J. Olson, AutoDock Vina: improving the speed and accuracy of docking with a new
516   scoring function, efficient optimization, and multithreading. *J Comput Chem* **31**, 455-461
517   (2010).

518 34.   N. M. O'Boyle *et al.*, Open Babel: An open chemical toolbox. *J Cheminform* **3**, 33 (2011).

519 35.   T. Hou, J. Wang, Y. Li, W. Wang, Assessing the performance of the MM/PBSA and MM/GBSA
520   methods. 1. The accuracy of binding free energy calculations based on molecular dynamics
521   simulations. *J. Chem. Inf. Model.* **51**, 69-82 (2010).

522

523

524

525

526
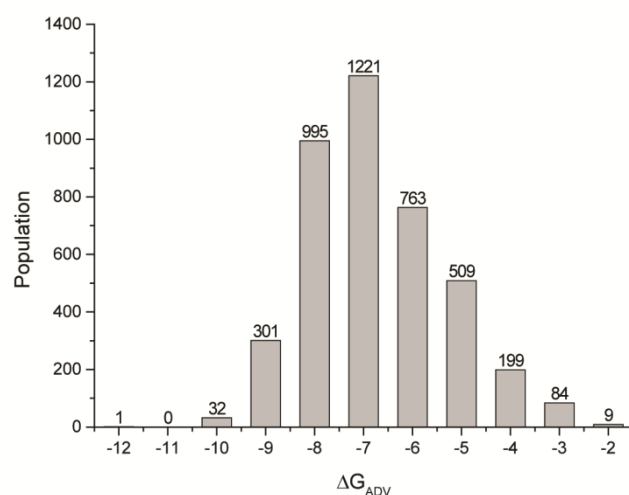
Extended Data Fig. S1. Virtual screening of small molecule compound library against GPcl. Bars represent numbers of
compounds with predicted free energies of binding in the indicated 1 kcal mol-1 bins.

529

530

531
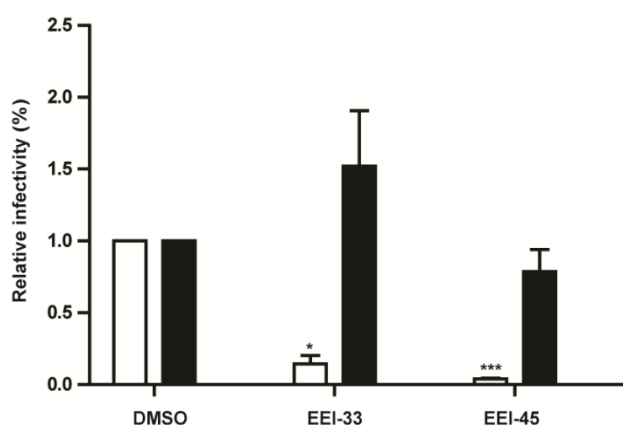
Extended Data Fig. S2. Inhibition of EBOVpp and VSVpp infection by EEI-33 and EEI-45. HEK293T cells were infected
with viruses EBOVpp (white bar) or VSVpp (black bar) in the presence of EEI-33 or EEI-45 at the final concentration of 10
μM. Data shown are the means ± s.d. n = 3. Value of the control is arbitrarily set as 1.

535

536

537

538

539

540

GPcl–EEI-20

| Compound	KD (M)	KD Error	$k_{on}(M^{-1}S^{-1})$	$k_{dis}(S^{-1})$	Full R^2
EEI-20	2.29E-04	6.99E-05	1.19E+04	2.73E+00	0.98

Extended Data Fig. S3. EEI-20 interacts with Ebola GPcl. Representative association and dissociation sensorgrams of EEI-20 binding to EBOV-GPcl. Values of KD, KD Error, kon, kdis, and R2 are shown.
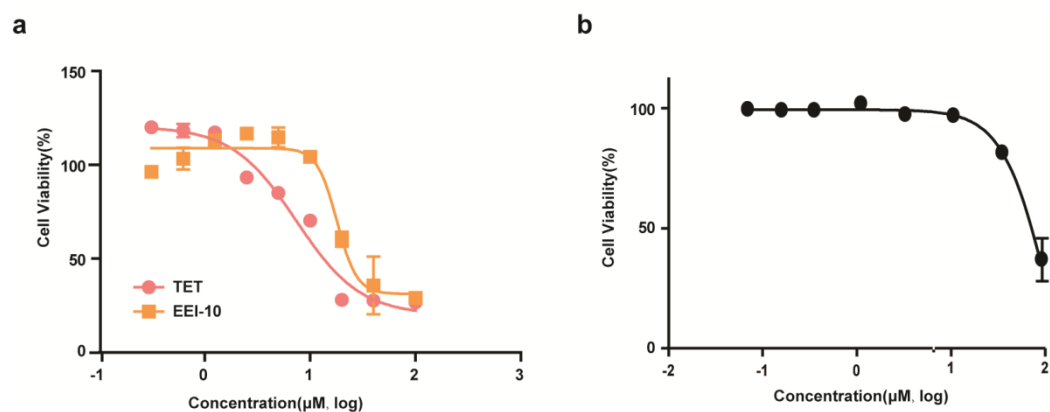
Extended Data Fig. S4. Cytotoxic effects of EEI-10 and TET on HEK293T cells. HEK293T (a) or Vero E6 (b) cells were incubated with EEI-10 or TET at different concentrations. The cell viability was analyzed by CCK8 assay. Data shown are the means ± s.d. n = 3.
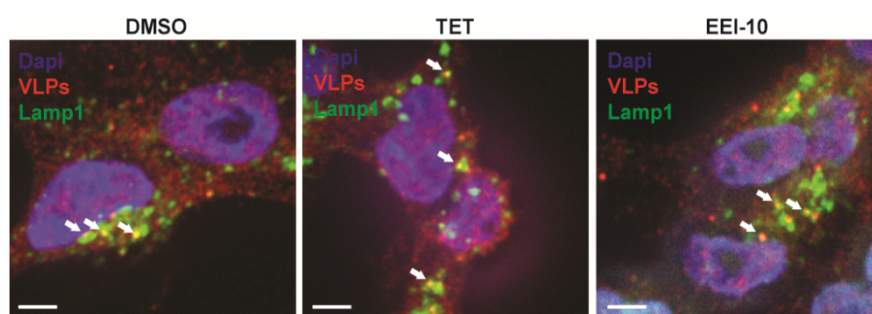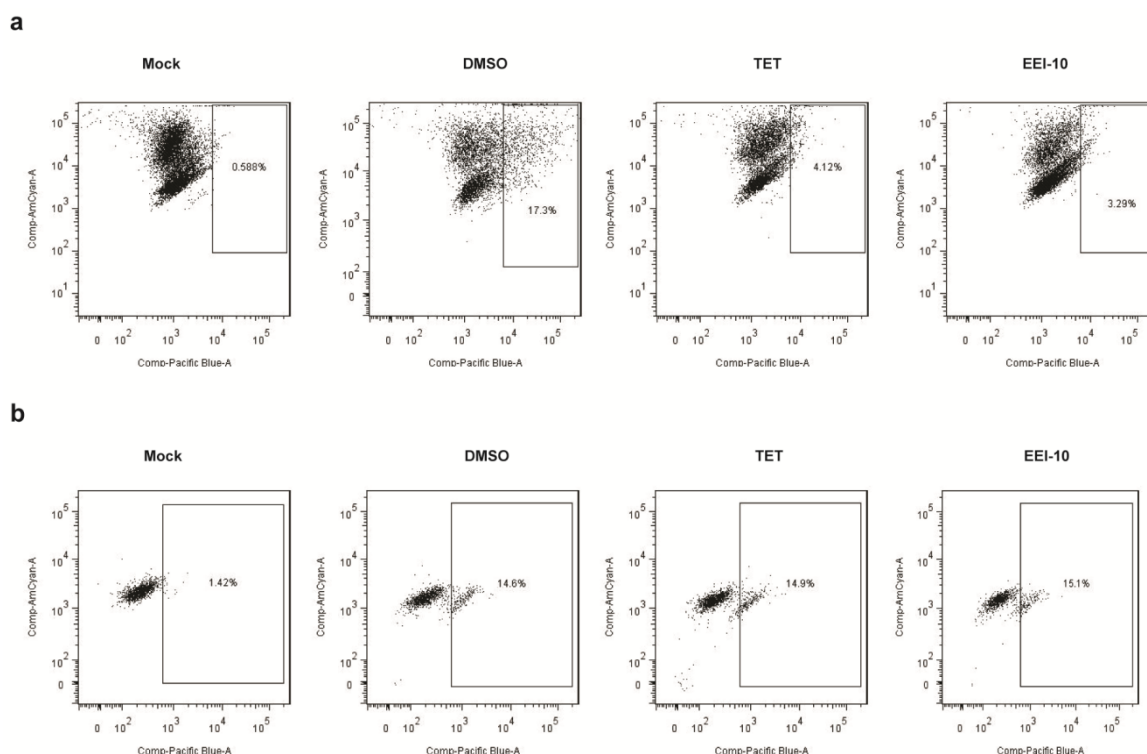
Extended Data Fig. S5. EEI-10 does not affect the transport of Ebola virus to late endosomes. HEK293T cells were incubated with Ebola VLPs for 4 hours in the presence of EEI-10 or TET. Colocalization of Ebola VLPs (in red) with Lamp1 (in green) was determined by confocal microscopy. Arrowheads indicate the colocalized VLPs and Lamp1. Scale bars, 5 μm.

Extended Data Fig. S6. EEI-10 inhibits EBOV GP-mediated membrane fusion. a, HeLa cells were infected with EBOVpp loaded with BlaM-Vpr in the presence of EEI-10. Release of virus capsid was determined by measuring cytoplasmic β-lactamase activity using the CCF4-AM Kit. Results shown are the representative FACS data of three independent experiments. b, BlaM-Vpr assay was performed to measure the effect of EEI-10 on VSVpp capsid release by infecting the HEK293T cells.

a

b

571
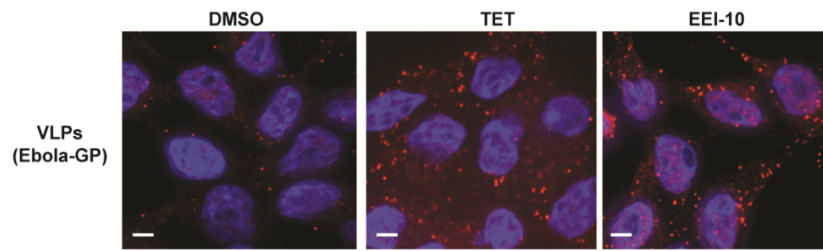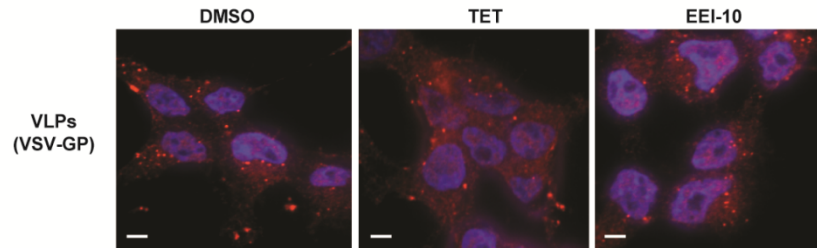
572   **Extended Data Fig. S7. EEI-10 causes accumulation of Ebola virus in the cytoplasm.** HEK293T cells were incubated with

573   Ebola-GP/HIV-luc (a) or VSV-GP/HIV-luc (b) under the treatment of EEI-10 or TET. Representative confocal images of virus

574   particles (in red) from three independent infection experiments are shown. Scale bars, 5 μm.

575

576

577

578
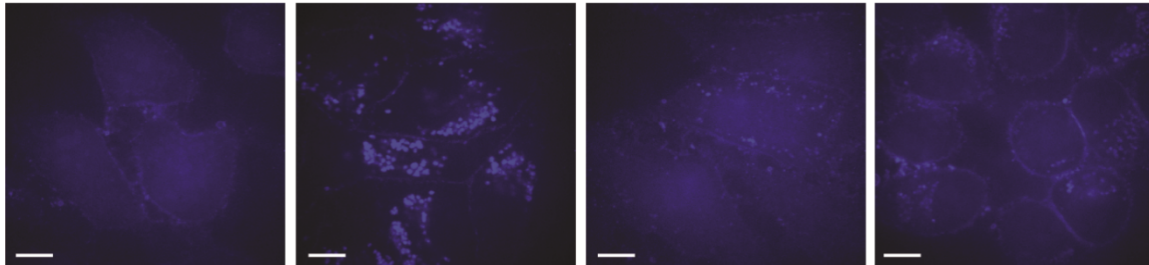
579   **Extended Data Fig. S8. EEI-10 does not affect the cholesterol transport.** HEK293T cells were treated with EEI-10 (5μM),

580   TET (5μM) or U18666A (5μM),   then stained with filipinⅢ (in blue). Representative confocal images are shown. Scale

581   bars, 5 μm.

582

583

584

585

586

587

Extended Data Fig. S9. Infectivity of EBOV GP mutants. HEK293T cells were infected with EBOVpp with Ebola GP (WT、T83A、E112A、I113A) at different dilutions for 48h, and viral infectivity were determined by measurement of luciferase activities, followed by calculation of viral titers. Data are mean ± s.d. n = 3.
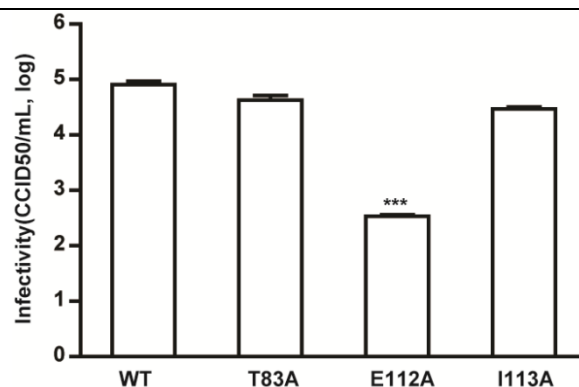
591

592 **Extended Data Table S1.** Information of the selected 46 compounds, including the predicted binding free energies (ΔG$_{ADV}$), TargetMol ID, CAS number, formula, and molecule weight (MolWt).

No.	ID	ΔG$_{ADV}$ (Kcal/mol)	CAS	Formula	MolWt
1	T1928	-10.2	875446-37-0	C30H25F10NO3	637.51
2	T0047	-8.7	357-57-3	C23H26N2O4	394.47
3	T0722	-9.2	77-52-1	C30H48O3	456.71
4	T0878	-9.4	520-27-4	C28H32O15	608.55
5	T1842	-10.4	1435488-37-1	C36H46N8O3	638.81
6	T2348	-10.2	1227911-45-6	C25H34N8O	462.59
7	T2585	-8.9	843663-66-1	C32H31BrN2O2	555.5
8	T2768	-8.7	20736-09-8	C42H68O13	780.99
9	T0049	-8.9	37091-65-9	C20H22N5NaO6S	483.47
10	T2920	-10.9	6078-17-7	C37H41ClN2O6	645.19
11	T0132	-9	33419-42-0	C29H32O13	588.56
12	T3122	-9.8	436-77-1	C37H40N2O6	608.74
13	T1304	-9.4	64-72-2	C22H23ClN2O8.HCl	515.35
14	T1138	-9.8	345909-26-4	C26H46NNaO8S	555.7

15	T0795	-8.7	153-18-4	C27H30O16	610.52
16	T2728	-9.7	1180-71-8	C26H30O8	470.52
17	T2830	-9.9	472-15-1	C30H48O3	456.71
18	T0595	-8.6	10236-47-2	C27H32O14	580.54
19	T2755	-8.7	17306-46-6	C27H30O14	578.52
20	T0125	-8.8	56390-09-1	C27H30ClNO11	579.98
21	T0171	-10.8	68-23-5	C20H26O2	298.42
22	T1521	-8.9	64439-81-2	C20H16N2O5	364.36
23	T6025	-9.6	850876-88-9	C35H46FN5O9S	731.84
24	T1213	-8.9	59703-84-3	C23H26N5NaO7S	539.54
25	T2831	-9.2	475-31-0	C26H43NO6	465.63
26	T1541	-10.3	67392-87-4	C24H30O3	366.49
27	T1259	-9.2	22204-24-6	C34H30N2O6S	594.69
28	T1571	-9.4	50-27-1	C18H24O3	288.39
29	T0129	-10.2	5578-73-4	C20H14ClNO4	367.79
30	T1832	-9.7	878419-78-4	C14H10F3N5O2	337.26
31	T1157	-10.8	113507-06-5	C37H53NO8	639.84
32	T2866	-10.5	510-30-5	C30H48O4	472.71
33	T1775	-9.4	1346572-63-1	C31H38N6O2	526.69
34	T2733	-10.2	126-19-2	C27H44O3	416.65
35	T2907	-9.2	568-73-0	C18H12O3	276.29
36	T1743	-10.1	170729-80-3	C23H21F7N4O3	534.43
37	T2239L	-8.8	518048-05-0	C20H21FN6O5	444.42
38	T1101	-9.3	13614-98-7	C23H28ClN3O7	493.94
39	T2405	-10	178307-42-1	C22H24ClFN4	398.91
40	T2239	-8.8	871038-72-1	C20H20FN6O5.K	482.51
41	T1035	-9.3	520-26-3	C28H34O15	610.57
42	T0131	-12.2	481-49-2	C37H38N2O6	606.73

43	T1499	-10	164656-23-9	C27H30F6N2O2	528.53
44	T1220	-8.6	1239-45-8	C21H20N3.Br	394.32
45	T2100	-10.5	1138549-36-6	C27H27N7O2S	513.61
46	T2906	-9.4	568-72-9	C19H18O3	294.35

594

595

596

597

598

599

600 **Extended Data Table S2.** Calculation of the interaction energy between EEI-10 and amino resides of EBOV-GPcl.

Residue	van der Waals	Electrostatic	Polar Solvation	Non-Polar Solv.	TOTAL
G112	0.12	-3.73	1.10	-0.02	-2.54
T83	-3.04	-0.39	1.38	-0.43	-2.49
I113	-1.88	-0.46	0.32	-0.21	-2.22
V141	-1.29	-0.91	0.70	-0.16	-1.66
F88	-1.73	-0.16	0.77	-0.28	-1.41
L111	-1.10	-0.02	0.07	-0.12	-1.17
W86	-1.61	-0.21	1.14	-0.17	-0.85
V79	-0.78	0.05	0.00	-0.08	-0.81
P80	-1.12	-0.18	0.70	-0.20	-0.80
G143	-0.85	-0.24	0.58	-0.11	-0.61

601 [a]The total energy (kcal mol^{-1}) is the sum of that of van der Waals, Electrostatic, Polar Solvation, and Non-Polar Solvation.

602 The residues are ranked by the values of their total energy. The top 10 residues are shown.

603

604

605

606

607 **Extended Data Table S3.** Calculation of the interaction energy between EEI-10 and amino acid residues of MARV-GP1a.

Residue	van der Waals	Electrostatic	Polar Solvation	Non-Polar Solv.	TOTAL
I125	-1.54	-0.43	0.30	-0.21	-1.88
F72	-2.07	-0.54	1.26	-0.29	-1.64
S67	-2.66	0.04	1.52	-0.36	-1.46
L64	-1.62	-0.35	0.82	-0.26	-1.41
V97	-1.11	-0.15	0.11	-0.15	-1.31
I95	-0.98	-0.10	0.03	-0.09	-1.14
N129	-1.56	-1.36	2.23	-0.30	-0.99
A71	-0.92	-0.25	0.41	-0.12	-0.89
K68	-1.25	0.33	0.63	-0.23	-0.52
G127	-0.62	-0.03	0.31	-0.09	-0.43

608 [a]The total energy (kcal mol^{-1}) is the sum of that of van der Waals, Electrostatic, Polar Solvation, and Non-Polar Solvation.
609 The residues are ranked by the values of their total energy. The top 10 residues are shown.

610

611

612
613

614

615

616

617

618

619

620

621

622

623